

Competing magnetic fluctuations in γ -iron due to peculiarities of its electronic structure

P. A. Igoshchev,¹ A. V. Efremov,¹ A. A. Katanin,^{1,2} A. I. Poteryaev,^{1,3} and V. I. Anisimov^{1,2}

¹*Institute of Metal Physics, Russian Academy of Sciences, 620990 Ekaterinburg, Russia*

²*Theoretical Physics and Applied Mathematics Department,
Ural Federal University, 620002 Ekaterinburg, Russia*

³*Institute of Quantum Materials Science, 620107 Ekaterinburg, Russia*

(Dated: October 9, 2012)

Applying the local density and dynamical mean field approximations to paramagnetic γ -iron, we revisit a problem of theoretical description of its magnetic properties in a wide temperature range. We show that contrary to α -iron, the frequency dependence of the electronic self-energy has a quasiparticle form for both, t_{2g} and e_g states. The momentum dependence analysis of static magnetic susceptibility shows maximum near the wave vector $\mathbf{q}_X = (2\pi, 0, 0)$, in agreement with the experimentally observed antiferromagnetic state in γ -iron precipitates. This state is however found to closely compete with the states, characterized by magnetic wave vectors along the directions $\mathbf{q}_X - (\pi, \pi, \pi) - (3\pi/2, 3\pi/2, 0)$. From the analysis of the uniform magnetic susceptibility we find, that contrary to α -iron, the Curie-Weiss law is not fulfilled in a broad temperature range, although the inverse susceptibility is nearly linear in the moderate-temperature region (1200–1500 K). This non-linearity of the inverse uniform magnetic susceptibility in broader temperature range is due to the density of states peak located in the vicinity of the Fermi level. Based on the obtained momentum dependence of the susceptibility in the paramagnetic phase the exchange integrals are estimated. The obtained results allow us to ascertain the size of the correlation effects in γ -iron as weak to moderate and give evidence of close relation of γ -iron to the other weak itinerant antiferromagnets.

PACS numbers: Valid PACS appear here

I. INTRODUCTION

The problem of magnetism of iron attracts a lot of attention till now. Pure α -iron has body centered cubic crystal lattice and it is ferromagnetic at temperatures below Curie temperature 1043 K^{1–3}. In the temperature range between 1043 and 1183 K α -iron is paramagnetic. This most studied allotrope of iron becomes, however, unstable above 1183 K because of the structural phase transition to the γ -phase^{1,4}, which has a face centered cubic crystal structure^{2,3}. The theory of the α - γ structural transition is still under development. Recent investigations^{5–7} have shown important role of magnetic correlations for this transition. These observations are supported by the results, indicating presence of local magnetic moments in α -iron even above the magnetic transition temperature⁸.

In view of these observations, understanding of magnetic properties of γ -iron seems to be necessary. Experimentally, the temperature dependence of inverse magnetic susceptibility in γ phase has very weak slope, which cannot be determined to a good accuracy because of large spread of experimental data (see Refs. 9,10 and references therein). Curie-Weiss temperature extracted from a fit to experimental data is negative, $\theta_{CW} \simeq -3451$ K, and the corresponding magnetic moment is about $\mu_{CW} = 7.47\mu_B$ ¹⁰. Therefore, magnetic properties of γ -iron are very different from those of α -iron, for which the Curie-Weiss temperature $\theta_{CW} \simeq 1093$ K and the magnetic moment $\mu_{CW} = 3.13\mu_B$ ⁹. The particles of the size between 60 Å and 700 Å in precipitates of γ -iron in copper are

found to be antiferromagnetic with the Néel temperature between 46 and 67 K^{11–13}.

The large Wilson–Sommerfeld ratio $R_W = (\pi^2 k_B^2 \chi) / (3\mu_B^2 \gamma) \sim 25$, which can be deduced from the magnetic¹⁰ and calorimetric measurements¹⁴, points to the presence of strong ferromagnetic fluctuations and indicates that the (antiferro)magnetism in γ -iron is likely to be frustrated by the competing magnetic fluctuations. Recent analysis¹⁵ within the ab-initio spin spiral approach have also shown presence of long-range competing exchange interactions. Such an analysis assumes however the existence of the local magnetic moments and at the same time neglects electronic correlations.

In the present paper we perform LDA and LDA+DMFT calculations to investigate the origin of weak antiferromagnetism of γ -iron, dominating types of magnetic fluctuations and possibility of the local moment formation in this substance.

II. SPECTRAL PROPERTIES

We first consider the results obtained for γ -iron in LDA approximation. γ -iron crystallizes in a stable face centered cubic structure in temperature interval from 1183 K to 1667 K and it has the lattice parameter $a = 3.656$ Å at 1183 K^{2,3}. Band structure calculations have been carried out in LDA approximation¹⁶ within tight-binding linear muffin-tin orbital atomic spheres approximation (TB-LMTO-ASA) framework¹⁷. The von Barth-Hedin local

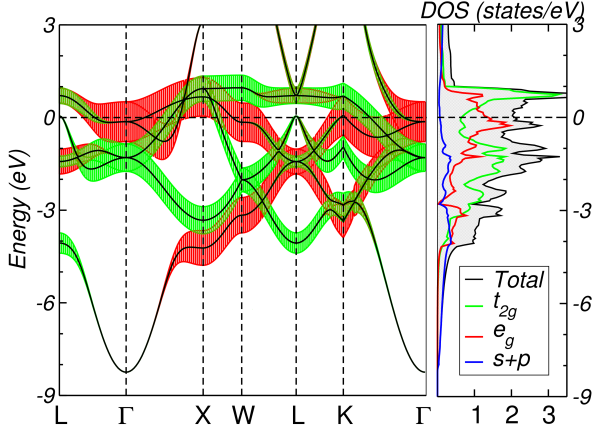


FIG. 1: (Color online) Left panel: the fatbands for t_{2g} and e_g orbitals in light (green) and dark (red) gray colors, respectively. Fatness corresponds to appropriate partial orbital contribution. Right panel: Iron density of states. Total DOS is shown by solid (black) line. Partial DOSes for t_{2g} , e_g and sum of $s + p$ orbitals are shown by light (green), dark (red) and dashed-dark (blue) gray lines, respectively.

exchange-correlation potential has been used¹⁸. Primitive reciprocal translation vectors have been discretized into 12 points along each direction which leads to 72 \mathbf{k} -points in irreducible part of the Brillouin zone.

The band structure together with the density of states are presented in the Fig. 1. On the left part of the figure the fatbands for the t_{2g} and e_g orbitals are shown by green and red colors, respectively (light and dark gray in the black-and-white version). The fatness coincides with the contribution of the corresponding partial DOSes shown on the right part of the Fig. 1. The bands of t_{2g} and e_g symmetries hybridize in the vicinity of the L point and in K- Γ direction. In other symmetry directions the t_{2g} and e_g manifolds hybridize weakly with s and p bands which span energy range from -8 eV to far above Fermi level (corresponding to zero energy). The t_{2g} states have a very flat region along X-W-L-K directions that is reflected in the DOS peak at 0.7 eV. At the Fermi level the partial t_{2g} DOS has a deep. Another large peaks of the t_{2g} DOS are located at -1.3 and -2.6 eV.

Although the e_g partial DOS has a bandwidth almost equal to the t_{2g} counterpart, its shape is very different. The corresponding dispersion has a flat part at small negative energy near Γ point (extended van Hove singularity, cf. Ref. 19), which results in the large peak of DOS just below the Fermi level at about -0.2 eV. This is in contrast to α -iron^{8,20}, where peak of e_g density of states is located very close to the Fermi level. As it will be shown below, this shift is of crucial importance for the magnetic properties difference between α - and γ -iron. The smaller peak of the corresponding partial DOS is located at -3.4 eV.

The Fermi surface obtained within LDA is shown in the Fig. 2. The four sheets that satisfy the equation for the

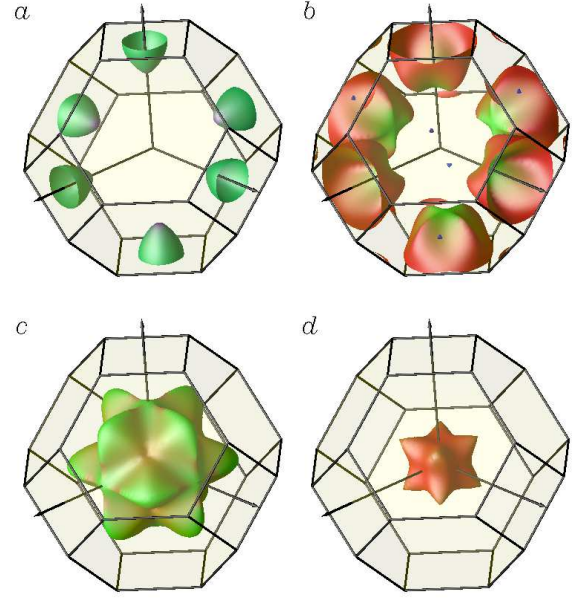


FIG. 2: (Color online) γ -iron Fermi surface sheets. The colorcoding reflects contribution of the orbital states. The (red,green,blue) scheme is used for the color definition of the point where red is for e_g , green is for t_{2g} and blue is for $s + p$ orbitals, respectively.

Fermi surface, $\varepsilon_{\mathbf{k}_F} = 0$, are colored such that amount of the appropriate color corresponds to the weight of partial contribution (we use the same colors as in Fig. 1: red for e_g states, green for t_{2g} states and blue for $s + p$ orbitals, respectively). The sheet *a* of the Fermi surface (Fig. 2a) is of mostly s , p , and e_g orbital characters. The sheets *b* and *c* (Figs. 2b,c) are mixture of t_{2g} and e_g characters. The last sheet *d* (Fig. 2d) consists mostly of e_g states. One should note that *b* and *c* sheets touch each other at the wavevector $(0.57, 0, 0)2\pi$ and thus lead to the three bands crossing the Fermi level along Γ -X direction (see Fig. 1). Near the touch point these sheets have a cross-like features perpendicular to $[0, 0, 1]$ direction with the small opposite incurvature produced by mostly t_{2g} states. This results in the approximate interband nesting of these crossed parts with close to zero wavevector and the intraband nesting with the wavevector $\mathbf{q}_A = (0.86, 0, 0)2\pi$. The *d* sheet reminds the cube stretched along diagonals and it has also the cross-like feature. Its existence allows one to consider two additional candidates for nesting vectors: within this sheet with $\mathbf{q}_B = (0.48, 0, 0)2\pi$ and the vector connecting the sheets *b, c* and *d*, $\mathbf{q}_C = (0.81, 0, 0)2\pi$.

In order to take into account correlation effects in 3d shell of γ -iron we apply the LDA+DMFT method (for detailed description of the computation scheme see Refs. 21,22). The Coulomb interaction parameter value, $U = 2.3$ eV, and the Hund's parameter, $I = 0.9$ eV, used in our work are the same as in earlier LDA+DMFT calculations by Lichtenstein *et al.*²³ for α -iron. The effec-

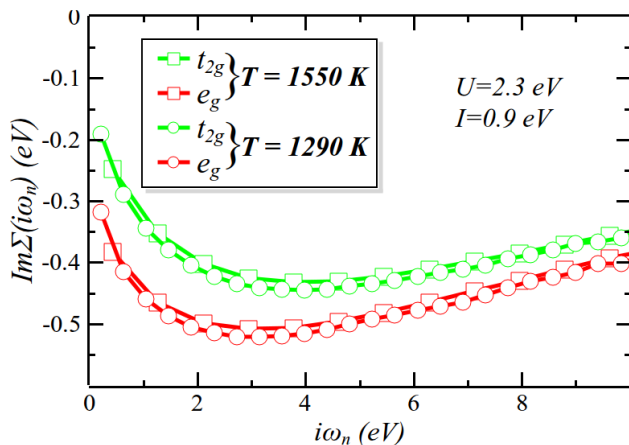


FIG. 3: (Color online) The imaginary parts of self-energies for t_{2g} (green) and e_g states (red) plotted on the Matsubara energy grid for different temperatures ($T=1290$ K — circles and $T=1550$ K — squares).

tive impurity model for DMFT was solved by quantum-Monte-Carlo (QMC) method with the Hirsch-Fye algorithm²⁴. Calculations were performed for the value of temperature $T \approx 1290$ K which is just above the α - γ structural transition temperature. Inverse temperature interval $0 < \tau < \beta \equiv 1/k_B T$ was divided in 100 slices. Four million QMC measurements were used in self-consistency loop within LDA+DMFT scheme and up to twelve million to refine data for spectral functions calculation with maximum entropy method²⁵.

The imaginary parts of self-energies for two values of temperature are presented in the Fig. 3. At low energies the behavior of the $\Im\Sigma(i\omega_n)$ is qualitatively similar for the t_{2g} and e_g orbitals. One can clearly see that increase of temperature does not change the frequency dependence qualitatively. The effective mass stays close to the bare value, $m^*/m=1.2$, and decreases slightly in temperature interval $1220 \text{ K} < T < 1550 \text{ K}$, where γ -iron exists in nature. One should note that the obtained imaginary part of e_g self-energy in γ -Fe has a quasiparticle-like frequency dependence, in stark contrast with the non-quasiparticle frequency dependence in α -phase⁸. This difference could be related to the peculiarities of the bare partial density of states near the Fermi level: the peak of partial DOS of e_g states in γ -iron is shifted from the Fermi level in comparison with α -iron down to -0.2 eV and the states at the Fermi energy lie at the slope of peak. The very similar situation is observed in iron-based superconductors²⁶.

Partial densities of states obtained in paramagnetic LDA+DMFT calculation for t_{2g} and e_g electrons are presented in Fig. 4. The LDA+DMFT densities of states are slightly narrower than the LDA counterparts implying weak correlation effects. This is in agreement with the small mass renormalization. One can observe that peak of e_g density of states obtained in LDA approach is broadened in LDA+DMFT calculation. The shape of

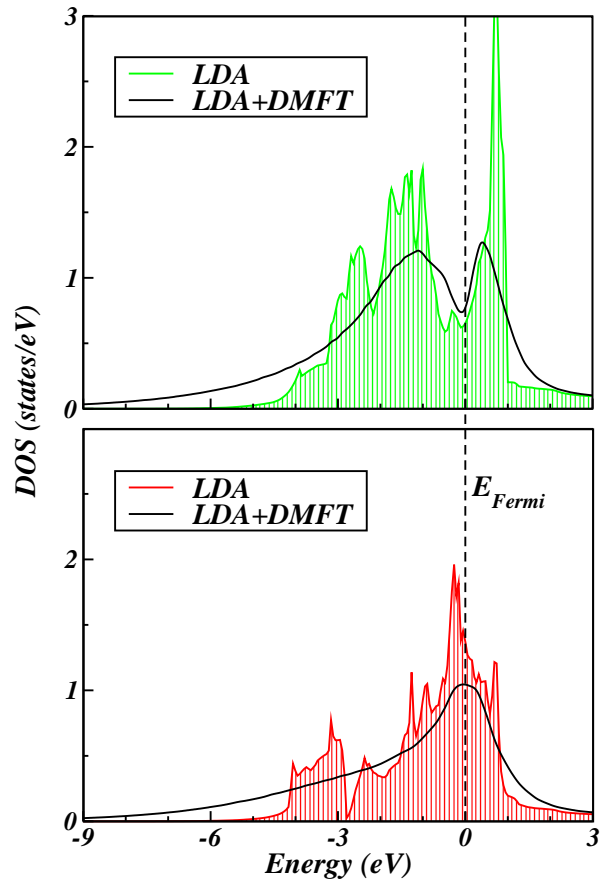


FIG. 4: (Color online) The iron t_{2g} (top panel) and e_g (bottom panel) partial density of states obtained within LDA+DMFT method (solid lines) compared with bare LDA PDOS (filled area).

t_{2g} density of states in LDA+DMFT approach resembles the LDA result with smearing of the peaky structures.

III. MAGNETIC PROPERTIES

To gain insight into favorability of different types of magnetic order in γ -iron, we analyze the momentum, \mathbf{q} , dependence of generalized static magnetic susceptibility $\chi_{\mathbf{q}}$ within LDA and LDA+DMFT approximations. The static magnetic susceptibility without correlation effects can be obtained as

$$\chi_{\mathbf{q}}^0 = -\frac{2\mu_B^2}{\beta} \sum_{\mathbf{k}, \omega_n} \text{Tr} [\mathcal{G}_{\mathbf{k}}^{\text{LDA}}(i\omega_n) \mathcal{G}_{\mathbf{k}+\mathbf{q}}^{\text{LDA}}(i\omega_n)], \quad (1)$$

where the Green function $\mathcal{G}_{\mathbf{k}}^{\text{LDA}}(i\omega_n) = (i\omega_n - \mathcal{H}_{\mathbf{k}} + \mu)^{-1}$, μ is the chemical potential and $\mathcal{H}_{\mathbf{k}}$ is the LDA-constructed Hamiltonian. Note that the temperature in Eq. (1) is introduced via the Fermi distribution function only. To analyze the contribution of different orbitals to

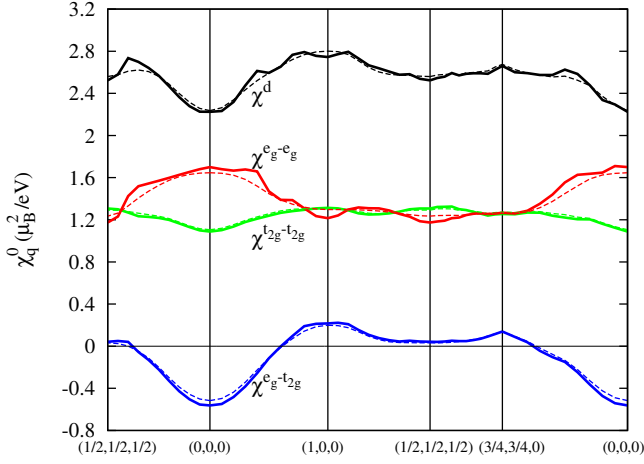


FIG. 5: (Color online) Contributions of different orbitals to magnetic susceptibility calculated according to the Eq. (5) in high symmetry directions. Black line corresponds to $\chi_q^{0,d}$. Red, green and blue lines show χ_q^{0,e_g-e_g} , $\chi_q^{0,t_{2g}-t_{2g}}$ and $\chi_q^{0,e_g-t_{2g}}$, respectively. Solid (dashed) lines correspond to $T=0$ ($T=1290$ K). Wavevectors are measured in units of 2π .

the susceptibility, we represent Green function

$$G_{\mathbf{k}}^{\text{LDA}}(i\omega_n) = \sum_{\alpha m_1 m_2} |m_1\rangle \frac{\bar{\psi}_{\mathbf{k}}^{\alpha m_1} \psi_{\mathbf{k}}^{\alpha m_2}}{i\omega_n - \varepsilon_{\alpha \mathbf{k}}} \langle m_2|, \quad (2)$$

where $\{|m\rangle\}$ is an orbital (LMTO) basis and $\psi_{\mathbf{k}}^{\alpha m}(\varepsilon_{\alpha \mathbf{k}})$ are LDA eigenvectors (eigenvalues) written in orbital representation (α is a band index). In this notation the equation (1) can be rewritten as

$$\chi_q^0 = -\frac{2\mu_B^2}{\beta} \sum_{\mathbf{k}n} \sum_{\substack{\alpha_1, \alpha_2 \\ m_1, m_2}} \frac{\bar{\psi}_{\mathbf{k}}^{\alpha_1 m_1} \psi_{\mathbf{k}}^{\alpha_1 m_2} \bar{\psi}_{\mathbf{k}+\mathbf{q}}^{\alpha_2 m_2} \psi_{\mathbf{k}+\mathbf{q}}^{\alpha_2 m_1}}{(i\omega_n - \varepsilon_{\alpha_1 \mathbf{k}})(i\omega_n - \varepsilon_{\alpha_2 \mathbf{k}+\mathbf{q}})}. \quad (3)$$

For the following analysis we split the susceptibility as

$$\chi_q^0 = \chi_q^{0,d} + \chi_q^{0,\text{rest}} \quad (4)$$

where the first term, $\chi_q^{0,d}$, corresponds to restricting the $m_{1,2}$ sum in Eq. (3) over d -orbitals only, while the second term, $\chi_q^{0,\text{rest}}$, contains the rest. This separation can be repeated further to analyze contributions to $\chi_q^{0,d}$ from different orbitals:

$$\chi_q^{0,d} = \chi_q^{0,e_g-e_g} + \chi_q^{0,t_{2g}-t_{2g}} + \chi_q^{0,e_g-t_{2g}}. \quad (5)$$

The results of such decomposition are presented in the Fig. 5. The intra-orbital contributions to the susceptibility at zero temperature, χ_q^{0,e_g-e_g} and $\chi_q^{0,t_{2g}-t_{2g}}$, are of the same magnitude and varying in “counter-phase” and thus compensating to large extent the \mathbf{q} dependence of each other. The $e_g - e_g$ contribution has weak momentum dependence, favoring ferromagnetic ordering (maximum at Γ point) and features at the nesting wavevectors

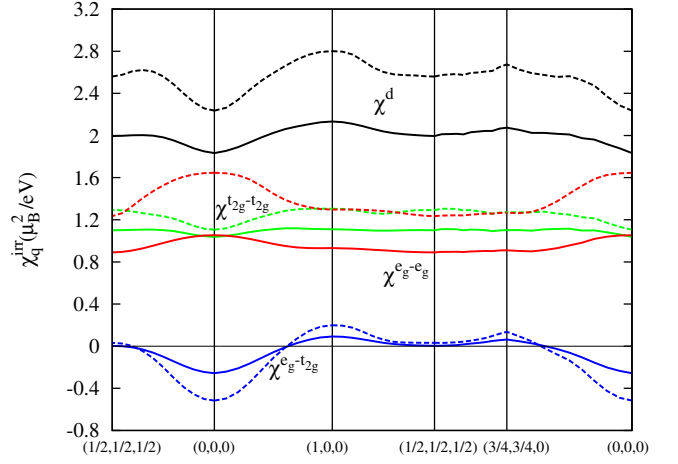


FIG. 6: (Color online) Contributions of different orbitals to irreducible susceptibility calculated according to the Eq. (1) (dashed lines) and in LDA+DMFT approach (Eq. (7), solid lines) in high symmetry directions at $T=1290$ K. Colorcoding and units repeats the previous picture.

\mathbf{q}_B and \mathbf{q}_C , discussed in Sec. II. Note that the magnetic behavior of e_g orbitals is very sensitive to the temperature, which is related to the peculiarities of the e_g band dispersion (the flatness of the spectrum along the direction Γ –L and the small size of the d sheet of the Fermi surface, see Fig. 2d). The momentum dependence of $t_{2g} - t_{2g}$ contribution is almost negligible and has a maximum at the wavevector $\mathbf{q}_X = (2\pi, 0, 0)$, related to the intraband nesting of the c Fermi surface sheet. The largest part of the momentum dependence of susceptibility comes from $e_g - t_{2g}$ contribution, which, at zero temperature, is maximal at the point \mathbf{q}_A and negative and large by magnitude in the vicinity of $\mathbf{q} = 0$ point due to small momentum transfer between electron-like (mainly t_{2g} -derived) Fermi-surface sheet c and hole-like (mainly e_g -derived) sheet b . The maximum of the resulting susceptibility $\chi_q^{0,d}$ is obtained close to the wavevector \mathbf{q}_A . Increasing temperature shifts maximum of $e_g - t_{2g}$ contribution, together with the maximum of the d -orbital susceptibility to the wave vector \mathbf{q}_X , stabilizing even further the antiferromagnetic fluctuations. The wave vector \mathbf{q}_X of the maximum of susceptibility corresponds to antiferromagnetic structure with alternating orientation of magnetic moments in adjacent layers of face-centered cubic crystal structure. This magnetic configuration was in fact observed in the precipitates of γ -iron²⁷.

The effects of electron-electron interaction can be treated within LDA+DMFT approach. Since, in general, interaction produces vertex correction to a single bubble considered above, we neglect for sake of simplicity the frequency dependence of these vertex corrections, introducing the frequency-independent vertex Γ^{irr} , such that

$$(\chi_q^0)^{-1} \rightarrow (\chi_q)^{-1} = (\chi_q^{\text{irr}})^{-1} - \Gamma^{\text{irr}}, \quad (6)$$

where

$$\chi_{\mathbf{q}}^{\text{irr}} = -\frac{2\mu_{\text{B}}^2}{\beta} \sum_{n,\mathbf{k}} \text{Tr} [\mathcal{G}_{\mathbf{k}}^{\text{DMFT}}(i\omega_n) \mathcal{G}_{\mathbf{k}+\mathbf{q}}^{\text{DMFT}}(i\omega_n)], \quad (7)$$

and

$$(\mathcal{G}_{\mathbf{k}}^{\text{DMFT}}(i\omega_n))^{-1} = (\mathcal{G}_{\mathbf{k}}^{\text{LDA}}(i\omega_n))^{-1} - \mathcal{P}_d \Sigma(i\omega_n) \mathcal{P}_d + \delta\mu. \quad (8)$$

$\Sigma(i\omega_n)$ is DMFT self-energy with subtracted double counting term, \mathcal{P}_d is a projector onto d -orbitals and $\delta\mu$ is a change of the chemical potential in DMFT with respect to LDA value.

Orbitally-resolved contributions to the irreducible susceptibility in LDA+DMFT approach are presented in the Fig. 6. One can see that the DMFT self-energy corrections lead to suppression of irreducible susceptibility, the momentum dependence becomes more flat in comparison to LDA, except the dip in the vicinity of the point $\mathbf{q} = 0$, which appear due to small momentum transfer processes between sheets b and c of the Fermi surface. The flat region implies close competition of the antiferromagnetic fluctuations with the wavevectors along the directions $\mathbf{q}_X - (\pi, \pi, \pi) - (3\pi/2, 3\pi/2, 0)$. According to the general ideas of spin-fluctuation theory²⁸, the weak momentum dependence of the irreducible susceptibility can be also attributed to the partial presence of local moments, discussed below.

To get further insight into the interplay of different magnetic fluctuations in γ -iron, we consider the uniform magnetic susceptibility; the latter can give a key for understanding the role of magnetic fluctuations. The uniform magnetic susceptibility $\chi(T)$ in the paramagnetic state of γ -iron was extracted from the LDA+DMFT simulations as a ratio of the induced magnetic moment by a small external magnetic field and the field magnitude^{26,29}. The temperature dependence of $\chi^{-1}(T)$ is presented on Fig. 7. We note the absence of fulfillment of the Curie-Weiss law

$$\chi(T) = \frac{\mu_{\text{CW}}^2}{3(T - \theta_{\text{CW}})}, \quad (9)$$

up to highest considered temperatures and the minimum of $\chi^{-1}(T)$ at $T^* \simeq 1000$ K. The effective magnetic moment, extracted from the slope of the inverse susceptibility in the low-temperature region (1200–1550 K), $\mu_{\text{CW}} = 5.75\mu_{\text{B}}$, is close to the experimentally observed value, $\mu_{\text{CW}} = 7.47\mu_{\text{B}}$ ^{9,10}. On the other hand, despite the Curie-Weiss law is not satisfied, roughly estimating the effective magnetic moment value, μ_{CW} , from high-temperature region (2500–4000 K) we find smaller value $\mu_{\text{CW}} \approx 4\mu_{\text{B}}$ (which approximately corresponds to spin $S = 3/2$).

In order to analyze the role of peculiarities of band structure on non-monotonous temperature behavior of $\chi(T)$, we calculate $\chi_{\mathbf{q}=0}^{\text{irr}}(T)$ projected onto pair sets of orbitals as in Eq. 5. The results are shown in Fig. 8 and inset of the Fig. 7. The overall temperature dependence of $\chi_{\mathbf{q}=0}^{\text{irr}}(T)$ repeats that of $\chi(T)$, being however

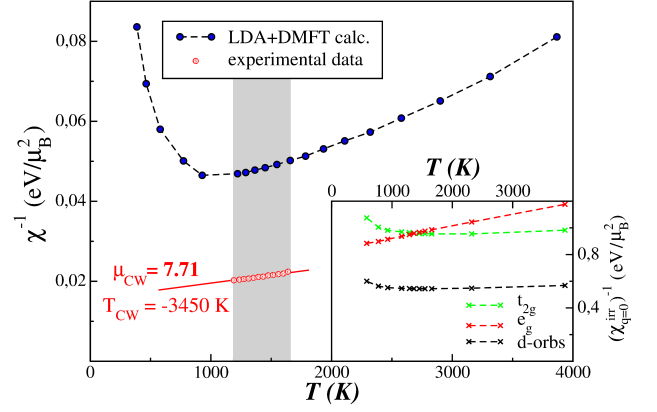


FIG. 7: (Color online) Temperature dependence of the inverse uniform magnetic susceptibility calculated within LDA+DMFT (blue circles) and experimental data⁹ (red circles), red line corresponds to the least square fit to Curie-Weiss law. Shadow covers the temperature range of γ -phase existence. Inset shows the inverse total (black) and orbital (red- e_g , green- t_{2g}) contributions to $\chi_{\mathbf{q}=0}^{\text{irr}}$.

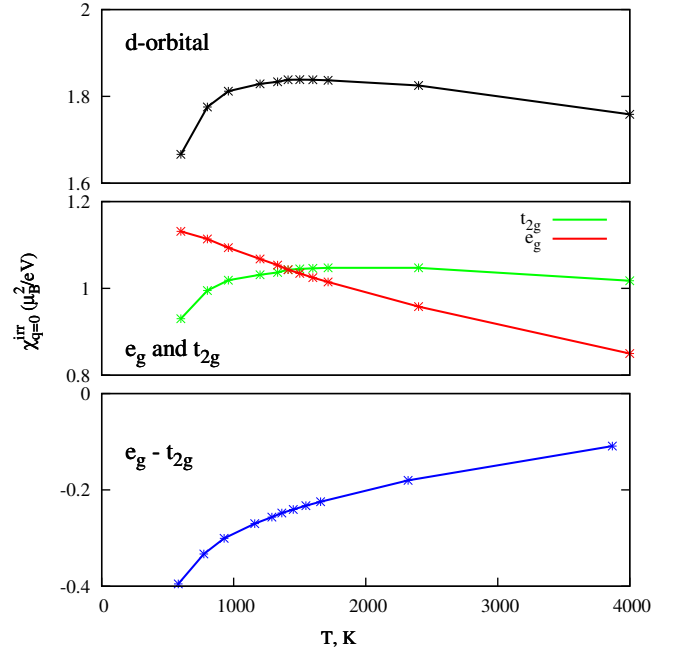


FIG. 8: (Color online) Temperature dependence of $\chi_{\mathbf{q}=0}^{\text{irr}}$ calculated within LDA+DMFT. Top panel – $\chi_{\mathbf{q}=0}^{\text{irr,d}}$, middle panel – $\chi_{\mathbf{q}=0}^{\text{irr,t2g}}$ and $\chi_{\mathbf{q}=0}^{\text{irr,e_g}}$, bottom panel – $\chi_{\mathbf{q}=0}^{\text{irr,e_g-t2g}}$.

substantially weaker. The t_{2g} contribution to $\chi_{\mathbf{q}=0}^{\text{irr}}$ has maximum at $T \sim 2000$ K, which originates from the maximum of t_{2g} -projected DOS above the Fermi level at the energy about 0.3 eV, similarly to pnictides²⁶. The e_g - t_{2g} contribution behaves similarly by magnitude at low enough temperature ($T < 1000$ K) but has a negative sign. The contribution of e_g orbitals decreases almost

linearly with increasing temperature. This is connected with strong (relatively to t_{2g} orbitals) correlated character of e_g orbitals. Such distinct behavior of different orbitals contributions results in the shift of maximum of total d -orbital irreducible susceptibility to approximately the temperature T^* , making it close to the position of uniform susceptibility maximum. We therefore interpret T^* as a crossover temperature which corresponds to the change of the dominating magnetic fluctuations. The ratio of total uniform susceptibility and irreducible one (Stoner enhancement factor) at $T \sim 1290$ K is about 10, which means that ferromagnetic fluctuations are strong in the temperature interval in the vicinity of T^* . Such a large ratio also explains strong temperature dependence of $\chi(T)$ in comparison with $\chi_{\mathbf{q}=0}^{\text{irr}}(T)$.

To investigate the possibility of the local moment formation in γ -iron the real part of the dynamic local magnetic susceptibilities for different temperatures have been calculated. In Fig. 9 we present these functions for different temperatures, rescaling both the susceptibility and frequency by temperature. For comparison, we also present on the inset the corresponding result for α -iron (see also Ref. 8). The dynamical mean-field theory, which neglects intersite magnetic exchange and therefore has no other low-energy scales apart from frequency and temperature, is expected to yield the local magnetic susceptibility, $\chi_{\text{loc}}(\omega) = (1/T)f(\omega/T)$, for the system with the local moments (where $f(x) \rightarrow 0$ at $x \rightarrow \infty$). Such a dependence also naturally provides the static nature of a single spin, $\chi_{\text{loc}} \propto \delta(\omega)$ at $T \rightarrow 0$. One can see that the susceptibility for α -iron obeys fully the above discussed scaling form, while for γ -iron some deviations from it are observed. The peak widths of the γ -iron susceptibilities are larger than those for α -iron, and the height of the peak (in units of $1/(k_B T)$) varies with temperature. Therefore the local moments in γ -iron are not well defined, which is also confirmed by the quasiparticle form of the self-energy obtained in Sect. II. However, the shape of the dependence $T\chi(\omega/T)$ changes only weakly with temperature allowing to estimate the size of the "effective" local moments from the values of static local susceptibility, $\mu_{\text{loc}}^2 = 3T\chi_{\text{loc}}(0)$. We obtain $\mu_{\text{loc}} \approx 3\mu_B$ in the temperature region 1200K-1400 K.

To estimate exchange interactions we perform the mapping of the considered electronic system to the effective Heisenberg model. Due to presence of different competing magnetic orders we consider a rough way to extract the exchange integrals using the electronic properties in the paramagnetic phase at finite temperature. To this end we compare a mean-field-like momentum dependence of the static magnetic susceptibility, $\chi_{\mathbf{q}}$, within the effective Heisenberg model with exchange parameters $J_{\mathbf{q}}$,

$$\chi_{\mathbf{q}} = \frac{\chi^0}{1 - J_{\mathbf{q}}\chi^0/(4\mu_B^2)}, \quad (10)$$

(where $\chi^0 = \chi^0(T) = \mu_{\text{loc}}^2/(3T)$), with the Eq. (6), which

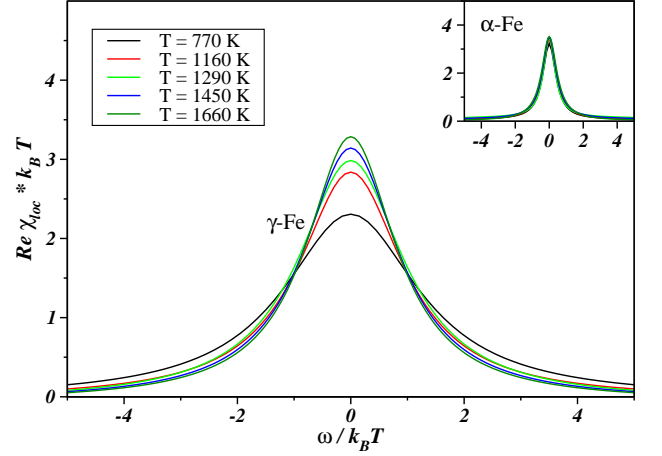


FIG. 9: (Color online) Local magnetic susceptibility of γ -iron for different temperatures. The inset shows the results for α -iron.

yields

$$J_{\mathbf{q}} = -4\mu_B^2 (\chi_{\mathbf{q}}^{\text{irr}})^{-1} + \text{const.} \quad (11)$$

Using the results for $\chi_{\mathbf{q}}^{\text{irr}}$ within the LDA+DMFT method one can obtain the constant in the Eq. (11) if one fix that $\sum_{\mathbf{q}} J_{\mathbf{q}} = 0$. At $T = 1290$ K we obtain $\min_{\mathbf{q}} J_{\mathbf{q}} = J_{\mathbf{q}=0} = -2380$ K and $\max_{\mathbf{q}} J_{\mathbf{q}} = J_{\mathbf{q}=\mathbf{q}_X} = 1172$ K, while for $T = 580$ K $\min_{\mathbf{q}} J_{\mathbf{q}} = J_{\mathbf{q}=0} = -5549$ K and $\max_{\mathbf{q}} J_{\mathbf{q}} = J_{\mathbf{q}=\mathbf{q}_X} = 1442$ K. Therefore, the exchange integrals with wavevectors near \mathbf{q}_X vary slightly with temperature, while the exchange $J_{\mathbf{q}=0}$ acquires strong temperature dependence, which implies that the local moment picture is better defined for magnetic states with the wavevectors near \mathbf{q}_X .

To estimate roughly the Néel temperature we consider the solution of mean-field-type equation

$$T_{\text{Néel}}^{\text{MF}} = \frac{(\mu_{\text{loc}}^2 J_{\mathbf{q}=\mathbf{q}_X})_{T=T_{\text{Néel}}^{\text{MF}}}}{3(2\mu_B)^2}, \quad (12)$$

performing linear interpolation for $J_{\mathbf{q}=\mathbf{q}_X}(T)$ and $\mu_{\text{loc}}^2(T)$ dependence. From this equation we obtain $T_{\text{Néel}}^{\text{MF}} = 793$ K. The Néel temperature is therefore strongly overestimated within our approach with respect to the experimental value. This agrees with the presence of strong frustration in γ -iron; the result (12) should be considered as an estimate for characteristic temperature of entering antiferromagnetic fluctuations-driven regime, which is of the same order of magnitude as T^* obtained above. Although the competition of different magnetic orders takes place already in the Heisenberg model on the face-centered cubic lattice³⁰ (making the mean-field treatment inadequate), it is expected to yield even stronger reduction of $T_{\text{Néel}}$ in itinerant system due to strong suppression of sublattice magnetization by paramagnons, having small gaps in their spectrum in the symmetric Brillouin zone points, different from $\mathbf{q} = \mathbf{q}_X$.

Considering analogously to weak itinerant ferromagnets the Rhodes-Wohlfarth ratio²⁸, $R = p_{\text{CW}}/p_s$, where $p_{\text{CW}} \approx 3.13$ is effective moment extracted from the Curie-Weiss law and $p_s = 0.75$ is a saturation moment, we obtain a large value $R \approx 4.17$, which is typical for itinerant but not the local moment magnets. This shows that in general γ -iron can be classified as a weak itinerant antiferromagnet with strong influence of the frustration effects.

IV. CONCLUSIONS

We have considered the electronic and magnetic properties of paramagnetic γ -iron. The shift of the DOS peak below the Fermi level in γ -iron causes the dramatic difference in the electronic and magnetic properties between α - and γ -iron. The position of this peak is therefore crucial for understanding the magnetic properties which is similar to recent study of pnictides²⁶. Other band structure features appear to be important for the antiferromagnetism of γ -iron, in particular, the e_g - t_{2g} hybridization favors to the nesting of Fermi surface. The obtained antiferromagnetic state with the wavevector close to $(2\pi, 0, 0)$ is found to compete strongly with the other incommensurate spin-density wave instabilities. Observed tendency

to the magnetic frustration can explain the small Néel temperature of γ -iron.

The account of correlation effects in γ -iron allows one to conclude that: *i)* the correlation strength is from moderate to weak; *ii)* the local moments are not well formed albeit the "effective" local moments can be introduced with $\mu_{\text{loc}} \approx 3\mu_B$ in the temperature range 1200K-1400 K. In general, γ -iron should be considered as a weak itinerant antiferromagnet with some importance of correlation effects.

The authors are grateful to Yu. N. Gornostyrev, A. V. Korolev, S. Wessel, A. N. Ignatenko and I. V. Leonov for useful discussions. This work was supported by the Russian Foundation for Basic Research (Projects Nos. 10-02-00046a, 12-02-91371-CT a, 10-02-91003-ANF a, 11-02-00931-a, 11-02-00937-a, 12-02-31510), the fund of the President of the Russian Federation for the support of scientific schools NSH-6172.2012.2, the Programs of the Russian Academy of Science: "Quantum microphysics of condensed matter" (No. 12-II-2-1002), "Strongly correlated electrons in solids and structures" (No. 12-T-2-1001), young scientist Project M-9; the grant of the Ministry of education and science of Russia No. 12.740.11.0026, the Program of "Dynasty" foundation.

-
- ¹ Z. S. Basinski, W. Hume-Rothery, and A. L. Sutton, Proc. R. Soc. London, Ser. A **229**, 459 (1955).
 - ² Constitution of Binary Alloys, edited by M. Hansen, McGraw-Hill, New York, 1958.
 - ³ J. Donohue, The Structure of the Elements, J. Wiley & Sons Ltd., New York, 1974.
 - ⁴ R. Kohlhaas, P. Dunner, N. Schmitz-Pranghle, Z. Angew. Phys. **23**, 245 (1967).
 - ⁵ S.V. Okatov, A.R. Kuznetsov, Yu.N. Gornostyrev, V.N. Urtsev, M.I. Katsnelson, Phys. Rev. B **79**, 094111 (2009)
 - ⁶ I. Leonov, A. I. Poteryaev, V. I. Anisimov, D. Vollhardt, Phys. Rev. Lett. **106**, 106405 (2011);
 - ⁷ I. Leonov, A. I. Poteryaev, V. I. Anisimov, D. Vollhardt, Phys. Rev. B **85**, 020401 (2012).
 - ⁸ A. A. Katanin, A. I. Poteryaev, A. V. Efremov, A. O. Shorikov, S. L. Skornyakov, M. A. Korotin, V. I. Anisimov, Phys. Rev. B **81**, 045117 (2010).
 - ⁹ S. Araj, D. S. Miller, J. Appl. Phys. **31**, 986 (1960).
 - ¹⁰ M. C. Gao, T. A. Bennett, A. D. Rollett and D. E. Laughlin, J. Phys. D: Appl. Phys. **39**, 2890 (2006).
 - ¹¹ U. Gonser, C. J. Meehan, A. H. Muir, H. Wiedersich, J. Appl. Phys. **34**, 2373 (1963).
 - ¹² G. J. Johanson, M. B. McGirr, D. A. Wheeler, Phys. Rev. B **1**, 3208 (1970).
 - ¹³ C. M. Liu and R. Ingalls, J. Appl. Phys. **50**, 1751 (1979).
 - ¹⁴ K. P. Gupta, C. H. Cheng, and P. Beck: J. Chem Solids, **25**, 73 (1964).
 - ¹⁵ S.V. Okatov, Yu.N. Gornostyrev, A.I. Lichtenstein, and M.I. Katsnelson, Phys. Rev. B **84**, 214422 (2011).
 - ¹⁶ R. O. Jones and O. Gunnarsson, Rev. Mod. Phys. **61**, 689 (1989).
 - ¹⁷ O. K. Andersen and O. Jepsen, Phys. Rev. Lett. **53**, 2571 (1984).
 - ¹⁸ U. von Barth and L. Hedin, J. Phys. C **5**, 1629 (1972).
 - ¹⁹ S. V. Vonsovskii, M. I. Katsnelson, and A. V. Trefilov, Fiz. Met. Metalloved. **76** (3) 3 (1993); **76** (4), 3 (1993).
 - ²⁰ R. Maglic, Phys. Rev. Lett. **31**, 546 (1973).
 - ²¹ V. I. Anisimov, D. E. Kondakov, A. V. Kozhevnikov, I. A. Nekrasov, Z. V. Pchelkina, J. W. Allen, S.-K. Mo, H.-D. Kim, P. Metcalf, S. Suga, A. Sekiyama, G. Keller, I. Leonov, X. Ren, and D. Vollhardt, Phys. Rev. B **71**, 125119 (2005).
 - ²² F. Lechermann, A. Georges, A. Poteryaev, S. Biermann, M. Posternak, A. Yamasaki, and O. K. Andersen, Phys. Rev. B **74**, 125120 (2006).
 - ²³ A. I. Lichtenstein, M. I. Katsnelson, and G. Kotliar, Phys. Rev. Lett. **87**, 067205 (2001).
 - ²⁴ J. E. Hirsch and R. M. Fye, Phys. Rev. Lett. **56**, 2521 (1986).
 - ²⁵ A. Sandvik, Phys. Rev. B **57**, 10287 (1998).
 - ²⁶ S.L. Skornyakov, A.A. Katanin, V.I. Anisimov, Phys. Rev. Lett. **106**, 047007 (2011).
 - ²⁷ S. C. Abrahams, L. Guttman and J. S. Kasper. Phys. Rev. **127**, 2052 (1962).
 - ²⁸ T. Moriya, Spin fluctuations in itinerant magnets. Springer-Verlag, Berlin, Heidelberg, 1985.
 - ²⁹ A. S. Belozarov, A. I. Poteryaev, and V. I. Anisimov, Phys. Rev. B **85**, 045109 (2012).
 - ³⁰ A. N. Ignatenko, A. A. Katanin, and V.Yu.Irkhin, JETP Letters **87**, 615 (2008).